Physics-based deep learning in application to fluid flow modeling and medical images processing

Elena Kornaeva
Dept. of Information Systems and Digital Technologies
Orel State University
Orel, Russia
smkornaeva@gmail.com

Alexey Kornaev
Research Center for Artificial Intelligence
Innopolis University
Innopolis, Russia
a.kornaev@innopolis.ru

Ivan Stebakov
Dept. of Mechatronics, Mechanics, and Robotics
Orel State University
Orel, Russia
chester50796@yandex.ru

Nikita Litvinenko
Research Center for Artificial Intelligence
Innopolis University
Innopolis, Russia
n.litvinenko@innopolis.university

Yuri Kazakov
Dept. of Mechatronics, Mechanics, and Robotics
Orel State University
Orel, Russia
kazakyurii@yandex.ru

Bulat Ibragimov
Dept. of Computer Science
University of Copenhagen
Copenhagen, Denmark
bulat@di.ku.dk

***Abstract*—Artificial neural networks are potentially powerful tool for spatial functions approximation. In this paper we proposed a method for modelling the three-dimensional flows of non-Newtonian fluids. The method is based on minimization of the proposed power loss and fitting the stream function distribution. This allows to calculate the fluid velocity distribution, the strain and stress distributions and to solve a problem in hydrodynamics. The goal of the method is that it does not need a data set for training and uses a three-dimensional image of the flow domain as a mask with sizes of $N \times N \times N$. Meanwhile, the U-Net or some other network processes 3 images with sizes of $1 \times N \times N$ that correspond to the components of the unknown stream function, and minimizes the power loss. The method was tested with MRI and CT images of suprarenal and ascending aortas and with asymptotic task of fluid flow in a pipe. The error was up to 12% in comparison with the analytical solutions.**

***Index Terms*—physics-based machine learning, loss, convolutional neural network, U-Net, non-Newtonian fluid, calculus of variations, variational principle, hydrodynamics, hemodynamics, magnetic resonance imaging, computed tomography**

I. Introduction

The idea of taking the path of least resistance arose a long time ago, and people find its confirmation both in themselves and in the environment. Aristotle expressed this idea in his writings, Fermat used this idea to describe the law of refraction of light, and Maupertuis was the first to formulate the principle of least action in mechanics [1]. Mechanics of continua has a set of conservation laws that have the form of variational principles. Some of the boundary value problems of solving partial differential equations (PDEs) can be transformed into the variational problems [2], [3]. One of the main difficulties of applying direct methods of calculus of variations is associated with the approximation of unknown functions, especially functions of multiple variables. Obviously, the artificial neural networks may help resolve this difficulty [4]–[6].

Lagrange variational principle [2] allows modeling fluid flows, but it has the following limitations: 1) fluid is Newtonian; 2) the unknown functions and their first derivatives are fixed on the boundary; 3) both, static and kinematic boundary conditions are required to find the value of the external power; 4) inertial and mass forces are negligible.

In this work the generalized Lagrange variational principle is applied to resolve most of the limitations mentioned above. The limitation on the inertial forces is unsolved. The method of three-dimensional (3D) non-Newtonian fluid flow modelling is proposed. The method is data set free and it can be applied to a 3D image of the flow domain. The paper deals with medical applications of the method and the tasks of blood flow in vessels.

II. Related works

A. Physiological fluids flows modeling

Whole blood is a two-phase liquid, composed of cellular elements suspended in plasma. Whole blood is a non-Newtonian fluid and characterized as shear-thinning, viscoelasticity, yield stress and thixotropy behavior [7], [8]. Many experimental studies have shown that blood is a predominantly shear thinning fluid [9]–[12]. This means that blood viscosity decreases as shear rate increases. This behavior is typical for vessels of small size or in areas of stable recirculation, for example, in the venous system and parts of the arterial vasculature, where the geometry is changed and red blood cell aggregates become more stable. In different vessels, the shear rate can vary from a few 1/s to more than 1000 1/s [13], [14]. According to [8], [10] the manifestation of non-Newtonian properties of blood occurs in the range of shear rates from 1 to 200 1/s. Baskurt et al. [15] shown that blood exhibits pronounced non-Newtonian properties at shear rates up to 100 1/s, in the range from 100

TABLE I: Metrics of the proposed method for the test fluid with non-Newtonian properties.

Model type	Function	Constant of model
Cross [18], [19]	$\mu_\infty + \frac{\mu_0-\mu_\infty}{1+(\theta_0\xi)^{\theta_1}}$	$\theta_0 = 1.007$ $\theta_1 = 1.028$
Modified Cross [18], [19]	$\mu_\infty + \frac{\mu_0-\mu_\infty}{(1+(\theta_0\xi)^{\theta_1})^{\theta_2}}$	$\theta_0 = 3.736$, $\theta_1 = 2.406$, $\theta_2 = 0.254$
Carreau-Yasuda [16], [20]	$\mu_\infty + \frac{\mu_0-\mu_\infty}{(1+(\theta_0\xi)^{\theta_1})^{\frac{\theta_2-1}{\theta_1}}}$	$\theta_1 = 1.902$ $\theta_1 = 1.25$ $\theta_3 = 0.22$
Eyring-Powell [7], [21]	$\mu_\infty + \frac{(\mu_0-\mu_\infty)\sinh^{-1}(\theta_0\xi)}{\theta_0\xi}$	$\theta_0 = 5.383$

to 200 1/s normal values range from 4 to 5 mPa s. When the shear rate increases above 200 1/s, the blood viscosity does not change. Works [11], [12] present viscosity measurements for blood analogues of various concentrations, it is shown that in the range of shear rates from 1 to 100 1/s, the viscosity decreases, and after 100 1/s, the viscosity is constant. Blood is also characterized by a thixotropic behavior [12], [16]. Thixotropy is more pronounced at low shear rates with a long time scale. However, this effect appears to have a less important role in blood flow than other non-Newtonian effects such as shear thinning [7], [12]. Blood also demonstrates yield stress although there is a controversy about this issue [7], [16], [17]. Yield stress models can be useful to model blood flow in capillaries where flow at very low shear rates occurs [16], [17].

A simple example of a shear thinning blood model is the power low [7], [16], for which the viscosity function is given by:

$$\mu(\xi) = \theta_0 \xi^{\theta_1 - 1}, \tag{1}$$

where $\theta_0,\ \theta_1$ are the model parameters; $\theta_1 < 1$ for pseudo-plastic fluid; $\theta_0,\ \theta_1$ are different and depend on hematocrit and temperature. For example, for hematocrit values of 40% and temperature of $37 \circ C$, the values of the model parameters are $\theta_0 = 0.1147$, $\theta_1 = 0.801$ [7], respectively.

The shear thinning power law model is often used for blood, due to the analytical solutions easily obtained for its governing equations, but there is a shortcoming since it predicts an unbounded viscosity at zero shear rate and zero viscosity when $\xi \to \infty$, which is unphysical [7]. Other viscosity models are shown in Table I. The asymptotic viscosities $\mu_0 = \lim_{\xi\to 0}\mu(\xi)$ and $\mu_0 = \lim_{\xi\to\infty}\mu(\xi)$, at $37^\circ C$ and hematocrits ranging from 33–45 % are the following $\mu_0 = 0.056\ Pa{\cdot}s$ and $\mu_\infty = 0.00345\ Pa{\cdot}s$ [7].

B. Mathematical modeling of fluid flow

According to the classical approach in modeling, the flow of blood as a viscous fluid is described by the Navier-Stokes and continuity equations [22], [23], which tensor forms are:

$$\rho\frac{d\mathbf{V}}{dt} = \nabla{\cdot}\mathbf{T}_\sigma + \rho\mathbf{F}, \tag{2}$$

$$\nabla{\cdot}\,\mathbf{V} = 0, \tag{3}$$

where ∇ is the Hamiltonian with the components $\partial/\partial x_i$, $\cdot$ is the dot product for divergence, $\mathbf{T}_\sigma$ is the stress tensor with the components σ_{ij}, $(i, j = 1\ldots 3)$, ρ is the density, $\mathbf{F}$ is the body force (e.g. gravity or magnetic force), $\mathbf{V}$ is the velocity vector with the components v_i and t is the time variable.

The stress tensor components σ_{ij} can be expressed from the generalized Newtonian hypothesis [7], [24] taking into account the incompressibility condition (Eq. 3):

$$\mathbf{D}_\sigma = 2\mu\mathbf{D}_\xi,$$

where $\mathbf{D}_\sigma = [[\sigma_{ij}]]$ and $\mathbf{D}_\xi = [[\xi_{ij}]]$ are strain stress and strain rate deviators, the deviator of the strain rate tensor is equal to the strain rate tensor $\mathbf{D}_\xi = \mathbf{T}_\xi$.

There are many works on blood flow modeling, in which Eqs. (2, 3) are solved by various grid methods of computational fluid dynamics (finite difference method, control volumes, finite elements). Vimmr et all [25] obtained a numerical solution of the equations (2, 3) for a 3D coronary artery bypass model that includes both proximal and distal coronary artery bypass grafts. an injured native artery and a connected end-to-side shunt with a junction angle of 45. A cell-centered formulation of the final volume of the central explicit fourth stage of the Runge-Kutta stepwise scheme was applied. The authors obtained a solution for coronary arteries (Reynolds number Re=230) using the Carro-Yasuda model and a modified cross-viscosity model. The results showed that the distribution of velocities is relatively similar with the case of Newtonian flow. However, the shear stress values on the walls of the model show a significant increase in the proximal and distal anastomoses and within the bypass shunt for both generalized Newtonian models compared to the Newtonian flow. Bodnar et all [17] studied blood flow in an idealized axisymmetric stenosis and in a realistic stenosed carotid bifurcation vessel. Blood was treated as shear-thinning (with Modified Cross model) and viscoelastic fluid (with Oldroyd-B model). The boundary conditions at the inlet were set as the velocity for the known Poiseuille flow with a given flow rate. At the outlet Neumann's uniform conditions for all velocity components and constant pressure were applied. On the vessel walls no-slip conditions were prescribed. For the case of Oldroyd-B model homogeneous Neumann conditions were imposed for the components of the extra stress tensor at all boundaries. The numerical solutions of the Eqs. (2, 3) were obtained by a finite-volume space discretization on structure grids, and an explicit Runge–Kutta time integration scheme. Similar studies [19], [20] were performed using commercial CFD software.

Another approach to studying the characteristics of a fluid flow has been known for a long time as a fit problem based on the data of a physical experiment. However, due to the strong nonlinearity of the quantities under study, a

large number of measurements are required, which is often difficult. An alternative to obtaining a training data set can be the result of a CFD simulation. Approximation of non-linear quantities can be performed using Convolutional Neural Networks (CNN) [26]. As a loss function, the authors use MSE with L_2 regularization. The combination of CNNs and Long Short Term Memory (LSTM) networks shows good results in the study of unsteady flows [27], [28]. The authors also use MSE as a loss function. Kissas et al. [29] developed physics-informed neural networks to model blood flow in large and medium-sized vessels. Training data (vessel shape, velocity and pressure) were obtained from Doppler ultrasound velocimetry and MRI data. The MSE loss function has been supplemented with PDEs residual and boundary conditions. Despite recent advances, this approach has low interpretability and generalizability [30]. In addition, it remains to obtain a large number of calculated points for the data set, as well as the previously indicated problem with mesh generation for complex flow geometry [31].

The disadvantages of the above approaches can be solved as follows. The studied flow characteristics can be approximated by neural networks using a physically based loss function and setting boundary conditions. This allows us to get rid of the training sample. Thus, the problem of numerically solving the PDEs is reduced to a variational problem. Unlike classical methods of using special series, unknown functions are approximated by DNN. The approach to minimizing the loss function, which has a physical meaning, can be applied to the mechanics of solid [32] and deformable [3] bodies, as well as to fluid mechanics [33], [34]. Sun et al. [31] presented a similar approach to modeling without using of a training set. The authors used a multilayer perceptron (MLP) to approximate the pressure and velocity fields. The loss function, as in [35], was represented by the sum of the PDE residual of Eqs. (2, 3) with the addition of boundary and initial conditions. However, the authors showed that in this case there is no need for a training data. The authors called this approach surrogate modeling for fluid flows based on physics-constrained deep learning without simulation data. A similar work was presented by Li et al. [36]. A solution of the Reynolds equation in the region between two eccentric cylinders was presented. The pressure function and gap function were approximated by MLP. The loss function was presented as the sum of the residual of the finite difference Reynolds equation with the addition of boundary conditions. The boundary conditions in the loss function are presented as the MSE of the predicted values of the pressure function at the boundary with the given ones. Also, the MSE of the gap function was added to the loss function. Each term of the loss function was appropriately weighted. Except for boundary conditions an additional dataset was not used. The presented MLP for approximating the solution of the Reynolds equation, the authors called the physics-informed neural network. Cuomo et al. [37] presented a solution of Dirichlet problem for the Laplace equation. The constant heat flux was added as boundary condition, what allowed to determine, together with the unknown function, also the optimal domain. The authors presented a loss function in the form of several terms. The first term is the known functional, which extremal corresponds to the solution of the Laplace equation. The penalization term was added to the loss function which enforces the unknown function to vanish outside a compact region. The Dirichlet conditions were taken into account by additional terms in the form of MSE of the unknown function on the boundary.

(a) (b) (c)

Fig. 1: Segments of image volumes from VMR: suprarenal abdominal aorta of a 76-year-old male patient with infrarenal aortic aneurysm (a), ascending aorta of a 11-year-old healthy female patient (b), suprarenal abdominal aorta with superior mesenteric artery of a 30-year-old healthy male patient (c).

III. Data collection

The proposed method is data set free. Meanwhile, we evaluate our method using 3 medical image volumes from the Vascular Model Repository (VMR) [38]. This data set contains image data, pathlines, segmentations, models (see Fig. 2), inflow rates, and simulation results for a range of large blood vessels. All segmentations, models, and simulation results were created in SimVascular [39] and verified by clinical experts.

Image volumes in VMR have anisotropic pixel spacing, so we resampled some volumes with the same spacings in all directions and selected 3 suitable volumes containing different aortic segments from patients of different ages, sex and health conditions to evaluate our method (see Fig. 1).

IV. Mathematical modeling

A. Variational formulation and the loss formalization

The paper deals with hydrodynamics. It is supposed that fluid is incompressible and the flow is laminar and steady. Since incompressibility is a natural property of fluids, the laminarity and stationarity of flows are typical assumptions in hydrodynamics [40] and in calculus of variations [1], respectively.

Some of the physical laws have variational formulation: *among all admissible functions, the proper function corresponds to the extremum value of the target functional*. In this work, it is necessary to find a kinematic function that characterizes the velocity distribution in the flow domain and minimizes a power functional.

In the previous work [34], the generalized Lagrange variational principle was proposed as the power functional for non-Newtonian fluids:

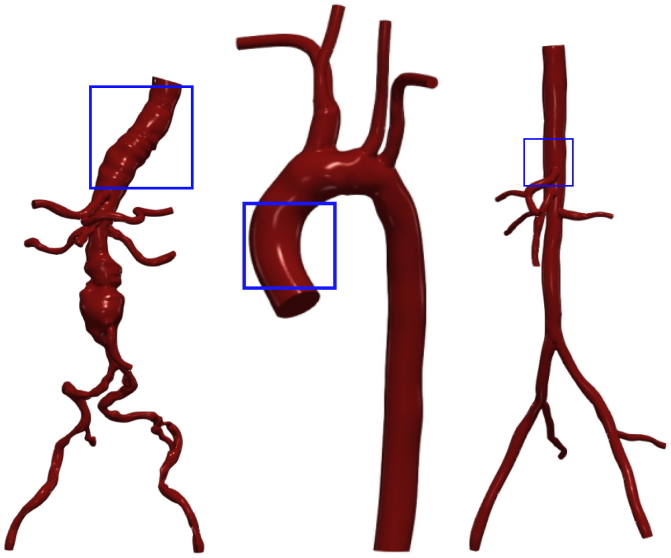

(a) (b) (c)

Fig. 2: Image volumes from VMR [38] with designated areas of interest: suprarenal abdominal aorta (a), ascending aorta (b), suprarenal abdominal aorta with superior mesenteric artery (c).

$$J_L^*[\mathbf{\Psi}] = \int_\Omega \Pi_v d\Omega \to min, \tag{4}$$

where $\mathbf{\Psi} = [\psi_i(x_j)]$ is the unknown stream function $(i, j = 1, 2, 3)$, Ω is the flow domain $(x_i^- \le x_i \le x_i^+)$ with surface S that is characterized by a unit outer normal vector $\boldsymbol{n}$, $\Pi_v = \int T dH$ is the viscoelastic potential, T is the shear stress intensity, H is the shear strain rate intensity.

The principle (4) was proved under the following constraints:

- each component of the unknown function depends on two coordinates $\mathbf{\Psi} = [\psi_1(x_2, x_3), \psi_2(x_1, x_3), \psi_3(x_1, x_2)]$;
- the non-Newtonian properties of the fluid are satisfied by the Herschel-Bulkley model [41], [42];
- the unknown $\mathbf{\Psi}$ function and its first partial derivatives are fixed on the surface S of the flow domain Ω.

The last point is equivalent to the boundary conditions [1], and it may have some alternative formulations [34].

The integrand (4) can be expressed in terms of the unknown $\mathbf{\Psi}$ function. The shear strain rate intensity H [1]:

$$H = \sqrt{2\xi_{ij}\xi_{ij}}, \tag{5}$$

depends on the components of the strain rate tensor $\mathbf{T}_\xi = [\xi_{ij}]$ that can be calculated using Cauchy's formula [23], [40], [43]:

$$\mathbf{T}_\xi = (\nabla \otimes \mathbf{V} + \mathbf{V} \otimes \nabla)/2, \tag{6}$$

where $\boldsymbol{V} = [v_i]$ is the velocity, $\nabla \otimes \mathbf{V}$ is the gradient of a vector function with components $\partial v_j / \partial x_i$.

[1]The Einstein summation notation is used in this work.

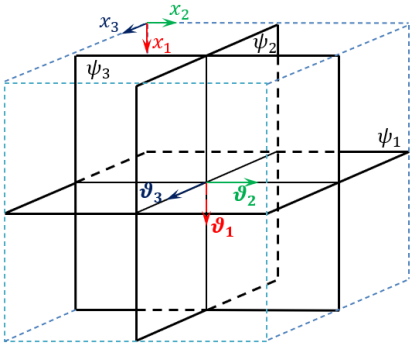

Fig. 3: The unknown stream function $\mathbf{\Psi}$ and the velocity function $\boldsymbol{V}$ (9) in the flow domain $(x_i^- \le x_i \le x_i^+)$.

The generalized Newtonian hypothesis is a rheological expression that allows connection of the statics and the kinematics of the fluid flow [7]:

$$T = \mu H, \tag{7}$$

where μ is the viscosity.

The Herschel-Bulkley law [41], [42] is taken into account in (4) as the rheological model of non-Newtonian fluids:

$$\mu(H) = q_0 + q_1 H^{z-1}, \tag{8}$$

where q_0, q_1, z are the parameters obtained from rheological tests.

Finally, the velocity $\boldsymbol{V}$ is a vorticity of the unknown $\mathbf{\Psi}$ function:

$$\mathbf{V} = \nabla \times \Psi. \tag{9}$$

In general, the 3D velocity distribution (9) depends on 3 2D scalar functions that are the components of the $\mathbf{\Psi}$ function. It should be noted, that the velocity distribution is solenoidal:

$$\nabla \cdot \boldsymbol{V} = \nabla \cdot (\nabla \times \mathbf{\Psi}) \equiv 0. \tag{10}$$

According to (10) the incompressibility condition [23], [43] is true, that makes any $\mathbf{\Psi}$ function kinematically admissible in the flow domain. The $\mathbf{\Psi}$ function is constrained on the surface S of the flow domain Ω. Since the flow rate can be expressed in terms of the stream function:

That allows to take the boundary conditions into account

B. Numerical differentiation and integration

The following templates are applied for the numerical differentiation...

The following methods are used for the numerical intergation...

V. Simulation Modeling

The proposed loss function (4) is general and can be applied for a three-dimensional flow (9) with unknown vector function $\mathbf{\Psi}$, and can be implemented by means of various approaches of simulation modeling. In general, the unknown $\mathbf{\Psi}$ function and its first partial derivatives should have fixed

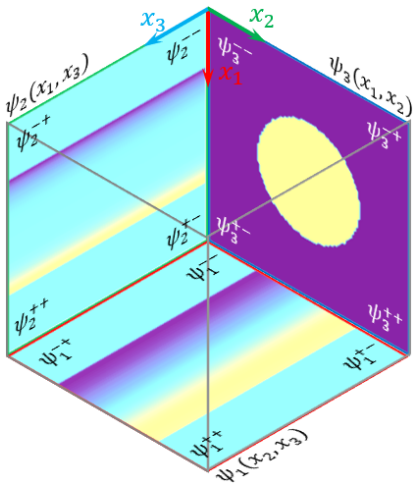

Fig. 4: The unknown stream function $\mathbf{\Psi}$ intuition and its values $\psi_i^{--}, \psi_i^{-+}, \psi_i^{+-}, \psi_i^{++}$ at the vertices of the the flow domain ($x_i^- \le x_i \le x_i^+$).

values on the surface of the flow domain. Alternatively, the limitations (**??**),(**??**) should be met.

Two approaches for the implementation of the proposed physics-based loss to steady incompressible fluid flow modeling are given below. The approaches differ in a kind of applied neural network and in the method of the flow domain representation.

A. Asymptotic case: Newtonian fluid flow through a pipe

It is supposed that the Newtonian fluid flows through a cylindrical pipe with radius R. The flow is laminar and steady, the Reynolds number is smaller than the critical one $Re < Re^*{\approx}1100...1400$ and the pipe length is greater than the critical one $L_3 > 0.16RRe$. Then the task is known as Poiseuille flow, and it has a simple analytical solution given in cylindrical coordinates $[\rho, \theta, x_3]$ [40]:

$$v_3 = -\frac{1}{4\mu}\frac{\partial p}{\partial x_3}(R^2 - \rho^2), \tag{11}$$

where $\partial p/\partial x_3$ is the pressure drop along the x_3 axis.

The flow rate trough the pipe cross section S_3 is equal to [40]:

$$Q_3 = \iint_{S_3} v_3 \rho \, d\rho \, d\theta = -\frac{\pi}{8}\frac{\partial p}{\partial x_3}\frac{R^4}{\mu}. \tag{12}$$

B. Multilayer perceptron and grid-based flow domain

The first proposed approach deals with .

C. Convolutional network and image-based flow domain

The network receives the data on the flow domain in a form of masked image of initial distribution of the unknown $\mathbf{\Psi}$ function. ...

The output of the network has the form of masked image for corrected distribution of the $\mathbf{\Psi}$ function. The following calculations with differenciations and integration operations should be done to calculate the loss and to finish the forward pass of the network.

For any given function $\mathbf{\Psi} = [\psi_i]$ that has fixed values on the boundaries of the flow domain together with its first, second, and third derivatives, the velocity distribution (9) can be expressed in compact or in expanded form, respectively:

$$\boldsymbol{V} = \left[\epsilon_{ijk}\frac{\partial \psi_k(x_i,x_j)}{\partial x_j}\right], \tag{13}$$

where ϵ_{ijk} is the Levi-Civita symbol [44],

$$\boldsymbol{V} = \left[\frac{\partial \psi_3}{\partial x_2} - \frac{\partial \psi_2}{\partial x_3}, \quad \frac{\partial \psi_1}{\partial x_3} - \frac{\partial \psi_3}{\partial x_1}, \quad \frac{\partial \psi_2}{\partial x_1} - \frac{\partial \psi_1}{\partial x_2}\right]. \tag{14}$$

It is convenient to present the flow domain Ω in the form of a parallelepiped (see Fig. 3). Then the flow rate through a cross-section $x_i = const$ can be expressed as follows:

$$Q_i(x_i) = -\epsilon_{ijk}(\psi_j(x_i, x_k^+) - \psi_j(x_i, x_k^-))l_j, \tag{15}$$

where $l_j = (x_j^+ - x_j^-)$.

The flow rates Q_i^-, Q_i^+ through 6 edges ($x_i = x_i^-, x_i = x_i^+$) should be given as a boundary conditions, and their sum should be zero in accordance with the fluid incompressibility condition. Taking (15) into account, the flow rate balance takes the following form:

$$\begin{aligned}
Q_1(x_1^-) &= -(\psi_2^{-+} - \psi_2^{--})l_2 + (\psi_3^{-+} - \psi_3^{--})l_3,\\
Q_1(x_1^+) &= -(\psi_2^{++} - \psi_2^{+-})l_2 + (\psi_3^{++} - \psi_3^{+-})l_3,\\
Q_2(x_2^-) &= -(\psi_3^{+-} - \psi_3^{--})l_3 + (\psi_1^{-+} - \psi_1^{--})l_1,\\
Q_2(x_2^+) &= -(\psi_3^{++} - \psi_3^{-+})l_3 + (\psi_1^{++} - \psi_1^{+-})l_1,\\
Q_3(x_3^-) &= -(\psi_1^{+-} - \psi_1^{--})l_1 + (\psi_2^{+-} - \psi_2^{--})l_2,\\
Q_3(x_3^+) &= -(\psi_1^{++} - \psi_1^{-+})l_1 + (\psi_2^{++} - \psi_2^{-+})l_2.
\end{aligned} \tag{16}$$

The system linear equations (18) is redefined since 6 equations have 12 unknowns. Some additional conditions are required. For example, it is permissible to suppose that the $\mathbf{\Psi}$ has constant values on some edges of the flow domain:

$$\psi_i^{-+} = \psi_i^{--}, \psi_i^{++} = \psi_i^{+-}. \tag{17}$$

The joined system of equations (18) and (17) is closed and the boundary values of the unknown function $\mathbf{\Psi}$ at the vertices of the flow domain can be determined if the values of the flow rates $Q_i(x_i^-)$, $Q_i(x_i^+)$ (18) through the edges of the flow domain $x_i = x_i^-$, $x_i = x_i^+$ are given.

Flow rates through the edges of the flow domain:

$$\begin{aligned}
Q_1(x_1^-) &= -(\psi_2^{-+})l_2,\\
Q_1(x_1^+) &= -(\psi_2^{++} - \psi_2^{+-})l_2,\\
Q_2(x_2^-) &= (\psi_1^{-+} - \psi_1^{--})l_1,\\
Q_2(x_2^+) &= (\psi_1^{++} - \psi_1^{+-})l_1,\\
Q_3(x_3^-) &= -(\psi_1^{+-} - \psi_1^{--})l_1 + (\psi_2^{+-} - \psi_2^{--})l_2,\\
Q_3(x_3^+) &= -(\psi_1^{++} - \psi_1^{-+})l_1 + (\psi_2^{++} - \psi_2^{-+})l_2.
\end{aligned} \tag{18}$$

It is convenient to suppose that $\psi_j(x_i, x_k^-) = 0$, then the flow rates through the edges S_i^+ are:

$$
\begin{aligned}
Q_1(x_1^-) &= -\psi_2(x_1^-, x_3^+)l_2 + \psi_3(x_1^-, x_2^+)l_3,\\
Q_1(x_1^+) &= -\psi_2(x_1^+, x_3^+)l_2 + \psi_3(x_1^+, x_2^+)l_3,\\
Q_2(x_2^-) &= -\psi_3(x_1^+, x_2^-)l_3 + \psi_1(x_2^-, x_3^+)l_1,\\
Q_2(x_2^+) &= -\psi_3(x_1^+, x_2^+)l_3 + \psi_1(x_2^+, x_3^+)l_1,\\
Q_3(x_3^-) &= -\psi_1(x_2^+, x_3^-)l_1 + \psi_2(x_1^+, x_3^-)l_2,\\
Q_3(x_3^+) &= -\psi_1(x_2^+, x_3^+)l_1 + \psi_2(x_1^+, x_3^+)l_2.
\end{aligned} \tag{19}
$$

Taking into account the symmetry of the shear rate tensor $\xi_{i,j} = \xi_{i,j}$, the tensor has the following form (6):

$$
\boldsymbol{T}_\xi = \frac{1}{2}\begin{bmatrix} 2\frac{\partial v_1}{\partial x_1}, & \frac{\partial v_1}{\partial x_2} + \frac{\partial v_2}{\partial x_1}, & \frac{\partial v_1}{\partial x_3} + \frac{\partial v_3}{\partial x_1} \\ \frac{\partial v_1}{\partial x_2} + \frac{\partial v_2}{\partial x_1}, & 2\frac{\partial v_2}{\partial x_2}, & \frac{\partial v_2}{\partial x_3} + \frac{\partial v_3}{\partial x_2} \\ \frac{\partial v_1}{\partial x_3} + \frac{\partial v_3}{\partial x_1}, & \frac{\partial v_2}{\partial x_3} + \frac{\partial v_3}{\partial x_2}, & 2\frac{\partial v_3}{\partial x_3} \end{bmatrix}. \tag{20}
$$

In the general case of a three dimensional flow the shear strain rate intensity H depends on all the components of the shear rate tensor:

$$
H = \sqrt{2(\xi_{11}^2 + \xi_{22}^2 + \xi_{33}^2 + 2\xi_{12}^2 + 2\xi_{13}^2 + 2\xi_{23}^2)}. \tag{21}
$$

Taking Newton's law of viscosity (7) and the Herschel-Bulkley law (8) into account, the loss (4) can be presented in the following form:

$$
J_L^* = \iiint_\Omega (\frac{q_0}{2}H^2 + \frac{q_1}{z+1}H^{z+1})\, dx_1\, dx_2\, dx_3. \tag{22}
$$

Among all admissible $\mathbf{\Psi}$ functions, the true one gives the loss (22) minimum value. It can be seen from (14), (20), (21), (22) that the loss (22) depends on the $\mathbf{\Psi}$ function and it can be determined by means of differentiation and integration operations. The network outputs the $\mathbf{\Psi}$ function in the discrete form of a three dimensional tensor and the elements of the tensor correspond to the intensities of 3D image pixels. So, numerical differentiation and integration should be met.

The unknown $\mathbf{\Psi}$ function in (**??**) is represented in the form of a three-dimensional tensor.

where Ω is flow domain (volume) with surface S that is characterized by a unit outer normal vector $\mathbf{n}$, $\Pi_v = \int T dH$ is viscoelastic potential, $T = \sqrt{s_{ij}s_{ij}/2}$ is shear stress intensity, $H = \sqrt{2\xi_{ij}\xi_{ij}}$ is shear strain rate intensity, σ^n is total external stress on the surface S.

VI. Results and discussion

The section deals with two approaches for the implementation of the proposed physics-based loss using machine learning and study some relatively simple problems in comparison with the known analytical or numerical solutions.

A. Multilayer perceptron and grid-based flow domain

The validation process of the model is represented by a numerical experiment with different values of hyperparameters. Table II presents a fragment of a computational experiment, the values of hyperparameters varied as follows $d = [1, 2, \dots 6]$, $l_{hid} = [10, 20, 30]$, $m = [20, 35, 50]$.

The experiment plan is a complete factorial experiment on the values of

TABLE II: Fragment of the validation results

degree	mean_error			
	$m = 20$		$m = 35$	
	$l_{hid} = 10$	$l_{hid} = 20$	$l_{hid} = 10$	$l_{hid} = 20$
1	0.3495	0.2887	0.2986	0.2746
2	0.0872	0.0827	0.0919	0.0828
3	0.0231	0.0230	0.0239	0.0240
4	0.0230	0.0230	0.0239	0.0239
5	0.0229	0.0230	0.0239	0.0239
6	0.0230	0.0230	0.0239	0.0238

B. Convolutional network and image-based flow domain

The previous subsection demonstrates that the proposed physics-based loss allow non-Newtonian fluid flows modelling.

TABLE III: Comparative simulation results

Method	Maximum velocity, m/s		
	parallel plates	***parallel plates with notch***	***nailfold capillary***
Analytical solution	7.5	-	-
Ansys Fluent	7.42	7.83	-
UNet with loss (**??**)	7.35	7.52	$8.8 \cdot 10^{-3}$

In the end of the section and the paper, the following advantages and disadvantages of the proposed grid-based and image-based approaches to solution of the CFD problems using ANNs in comparison with known methods in CFD should be highlighted.

Advantages.The proposed approaches are

- able to take into account the non-Newtonian properties of fluids and mass forces, e.g. magnetic force, gravity force;
- free of data sets at the training stage due to the proposed physics-based loss;
- easy in implementation, especially the image-based approach that solves a problem using an image as input;

Disadvantages. The proposed approaches are

- able to model stationary or quasi-stationary flows only;
- are time consuming and less accurate in comparison with ANSYS Fluent, at least at the present stage of using the simplest methods for approximation.

The model (4) has the following assumptions:

- able to model stationary or quasi-stationary flows only;
- are time consuming and less accurate in comparison with ANSYS Fluent, at least at the present stage of using the simplest methods for approximation.

The model (4) has the following prospects:

- able to model stationary or quasi-stationary flows only;
- are time consuming and less accurate in comparison with ANSYS Fluent, at least at the present stage of using the simplest methods for approximation.

VII. Conclusions

Complex flow domains with internal walls, porous media.

This research highlights the scope of non-Newtonian fluids flow modeling. The following conclusions should be made.

1. The proposed generalized Lagrange variational principle takes into account complex rheological properties of fluids and external body forces that allow modelling non-Newtonian and rheomagnetic fluid flows for a wide range of applications in engineering, medicine, chemistry etc. The principle is also less demanding of boundary conditions than the basic Lagrange principle.

2. The proposed generalized Lagrange functional performs a physics-based loss for machine learning algorithms. The loss minimisation does not require any data set and can be implemented in many ways. The paper demonstrates two approaches connected with grid-based and image-based flow domain representation. The second one allows modeling fluid flows using the flow domain image as input.

3. The proposed loss is mathematically justified and the obtained simulation modeling results demonstrated that the proposed algorithms are accurate enough. The algorithms can be generalized for the modeling of 3D non-Newtonian fluids flows. They also can be enhanced with more advanced methods of discretization and approximation, with application of other types of network architectures.

The authors suppose that the main prospect of the research is connected with medical applications and modeling of physiological fluid flows, including joints lubrication, blood circulation, and drug delivery tasks, using 2D and 3D images of the flow domains.

ACKNOWLEDGMENT

The authors express gratitude to the organizing committee of the IEEE 2023 Congress on Evolutionary Computation for the opportunity to discuss the results of the research, to the reviewers and the editors who helped to enhance the paper, and to Vera Panyushkina for the assistance with the translation of this paper.

AUTHORS CONTRIBUTION

Alexey Kornaev proposed Elena Kornaeva proposed in section 5 of the paper Nikita Litvinenko Ivan Stebakov Yuri Kazakov

CHECK LIST

- check if the paper is anonymous (authors, acknowledgements, contributions)
- check if there any italic Greek characters left
- read the text
- comment on this list

REFERENCES

[1] I. M. Gelfand and S. V. Fomin, *Calculus of Variations*, R. Silverman, Ed. Courier Corporation, 2000. [Online]. Available: https://books.google.com/books/about/Calculus_of_Variations.html?hl=ruid=YkFLGQeGRw4C

[2] R. S. Schechter and G. F. Newell, *The Variational Method in Engineering*. American Society of Mechanical Engineers Digital Collection, 3 1968, vol. 35.

[3] E. Samaniego, C. Anitescu, S. Goswami, V. M. Nguyen-Thanh, H. Guo, K. Hamdia, T. Rabczuk, and X. Zhuang, "An energy approach to the solution of partial differential equations in computational mechanics via machine learning: Concepts, implementation and applications," *Computer Methods in Applied Mechanics and Engineering*, vol. 362, 8 2019. [Online]. Available: http://arxiv.org/abs/1908.10407 http://dx.doi.org/10.1016/j.cma.2019.112790

[4] K. Hornik, M. Stinchcombe, and H. White, "Multilayer feedforward networks are universal approximators," *Neural Networks*, vol. 2, pp. 359–366, 1 1989.

[5] M. W. Dissanayake and N. Phan-Thien, "Neural-network-based approximations for solving partial differential equations," *Communications in Numerical Methods in Engineering*, vol. 10, pp. 195–201, 3 1994. [Online]. Available: https://onlinelibrary.wiley.com/doi/full/10.1002/cnm.1640100303

[6] N. Thuerey, P. Holl, M. Mueller, P. Schnell, F. Trost, and K. Um, *Physics-based Deep Learning*. WWW, 2021. [Online]. Available: http://physicsbaseddeeplearning.org

[7] A. Sequeira, *Hemorheology: Non-newtonian constitutive models for blood flow simulations*. Springer Verlag, 2018, vol. 2212, pp. 1–44.

[8] O. K. Baskurt, M. Boynard, G. C. Cokelet, P. Connes, B. M. Cooke, S. Forconi, F. Liao, M. R. Hardeman, F. Jung, H. J. Meiselman, G. Nash, N. Nemeth, B. Neu, B. Sandhagen, S. Shin, G. Thurston, and J. L. Wautier, "New guidelines for hemorheological laboratory techniques," *Clin. Hemorheol. Microcirc.*, vol. 42, pp. 75–97, 2009.

[9] R. Revellin, F. Rousset, D. Baud, and J. Bonjour, "Extension of murray's law using a non-newtonian model of blood flow," *Theor. Biol. Medical Model.*, vol. 6, 2009.

[10] M. M. Molla and M. C. Paul, "Les of non-newtonian physiological blood flow in a model of arterial stenosis," *Med. Eng. Phys.*, vol. 34, pp. 1079–1087, 2012.

[11] J. M. Jung, D. H. Lee, and Y. I. Cho, "Non-newtonian standard viscosity fluids," *Int. Commun. Heat Mass Transf.*, vol. 49, pp. 1–4, 2013.

[12] P. K. Mandal, "An unsteady analysis of non-newtonian blood flow through tapered arteries with a stenosis," *Int. J. Non-Linear Mech.*, vol. 40, pp. 151–164, 1 2005.

[13] E. Nader, S. Skinner, M. Romana, R. Fort, N. Lemonne, N. Guillot, A. Gauthier, S. Antoine-Jonville, C. Renoux, M. Hardy-Dessources, E. Stauffer, P. Joly, Y. Bertrand, and P. Connes, "Blood rheology: Key parameters, impact on blood flow, role in sickle cell disease and effects of exercise," *Front. Physiol.*, vol. 10, p. 1329, 2019.

[14] P. Connes, T. Alexy, J. Detterich, M. Romana, M. D. Hardy-Dessources, and S. K. Ballas, "The role of blood rheology in sickle cell disease," *Blood Reviews*, vol. 30, pp. 111–118, 3 2016.

[15] O. K. Baskurt and H. J. Meiselman, "Blood rheology and hemodynamics," *Semin. Thromb. Hemost.*, vol. 29, pp. 435–450, 2003.

[16] T. Sochi, "Non-newtonian rheology in blood circulation," pp. 1–26, 2013. [Online]. Available: http://arxiv.org/abs/1306.2067

[17] T. Bodnar, A. Sequeira, and M. Prosi, "On the shear-thinning and viscoelastic effects of blood flow under various flow rates," *Appl. Math. Comput.*, vol. 217, pp. 5055–5067, 2011.

[18] F. Abraham, M. Behr, and M. Heinkenschloss, "Shape optimization in steady blood flow: A numerical study of non-newtonian effects," *Computer Methods in Biomechanics and Biomedical Engineering*, vol. 8, pp. 127–137, 2005.

[19] Y. H. Kim, P. J. VandeVord, and J. S. Lee, "Multiphase non-newtonian effects on pulsatile hemodynamics in a coronary artery," *International Journal for Numerical Methods in Fluids*, vol. 58, pp. 803–825, 11 2008.

[20] C. Fisher and J. S. Rossmann, "Effect of non-newtonian behavior on hemodynamics of cerebral aneurysms," *Journal of Biomechanical Engineering*, vol. 131, 9 2009.

[21] J. Zueco and O. Beg, "Network numerical simulation applied to pulsatile," *Int. J. of Appl. Math and Mech.*, vol. 5, pp. 1–16, 2009.

[22] Y. Hori, *Hydrodynamic lubrication*. Tokyo: Yokendo Ltd, 2006.

[23] S. V. Patankar, *Numerical Heat Transfer and Fluid Flow*, 1st ed. CRC Press, 10 1980. [Online]. Available: https://www.taylorfrancis.com/books/mono/10.1201/9781482234213/numerical-heat-transfer-fluid-flow-suhas-patankar

[24] N. Kochin, I. Kibel', and N. Roze, *Theoretical hydromechanics*, J. Radok, Ed. Interscience Publishers, 1964.

[25] J. Vimmr, A. Jonasova, and A. Jonášová, "On the modelling of steady generalized newtonian flows in a 3d coronary bypass," *Engineering MECHANICS*, vol. 15, pp. 193–203, 2008. [Online]. Available: https://www.researchgate.net/publication/41956789

[26] X. Jin, P. Cheng, W. L. Chen, and H. Li, "Prediction model of velocity field around circular cylinder over various reynolds numbers by fusion convolutional neural networks based on pressure on the cylinder," *Physics of Fluids*, vol. 30, p. 047105, 4 2018. [Online]. Available: https://aip.scitation.org/doi/abs/10.1063/1.5024595

[27] R. Han, Y. Wang, Y. Zhang, G. C. P. of Fluids, and undefined 2019, "A novel spatial-temporal prediction method for unsteady wake flows based on hybrid deep neural network," *Physics of Fluids*, vol. 31, p. 127101, 12 2019. [Online]. Available: https://sci-hub.do/https://aip.scitation.org/doi/abs/10.1063/1.5127247

[28] P. A. Srinivasan, L. Guastoni, H. Azizpour, P. Schlatter, and R. Vinuesa, "Predictions of turbulent shear flows using deep neural networks," *Physical Review Fluids*, vol. 4, 5 2019.

[29] G. Kissas, Y. Yang, E. Hwuang, W. R. Witschey, J. A. Detre, and P. Perdikaris, "Machine learning in cardiovascular flows modeling: Predicting arterial blood pressure from non-invasive 4d flow mri data using physics-informed neural networks," *Computer Methods in Applied Mechanics and Engineering*, vol. 358, 1 2020.

[30] Y. Li, J. Chang, C. Kong, and W. Bao, "Recent progress of machine learning in flow modeling and active flow control," *Chinese Journal of Aeronautics*, vol. 35, pp. 14–44, 4 2022.

[31] L. Sun, H. Gao, S. Pan, and J. X. Wang, "Surrogate modeling for fluid flows based on physics-constrained deep learning without simulation data," *Computer Methods in Applied Mechanics and Engineering*, vol. 361, 4 2020.

[32] S. J. Raymond and D. B. Camarillo, "Applying physics-based loss functions to neural networks for improved generalizability in mechanics problems," 2021. [Online]. Available: https://arxiv.org/abs/2105.00075

[33] E. Kornaeva, A. Kornaev, and S. Egorov, "Application of artificial neural networks to solution of variational problems in hydrodynamics," *Journal of Physics: Conference Series*, vol. 1553, 5 2020.

[34] E. Kornaeva, A. Kornaev, A. Fetisov, I. Stebakov, and B. Ibragimov, "Physics-based loss and machine learning approach in application to non-newtonian fluids flow modeling," *2022 IEEE Congress on Evolutionary Computation, CEC 2022 - Conference Proceedings*, 2022.

[35] M. Aliakbari, M. Mahmoudi, P. Vadasz, and A. Arzani, "Predicting high-fidelity multiphysics data from low-fidelity fluid flow and transport solvers using physics-informed neural networks," *International Journal of Heat and Fluid Flow*, vol. 96, 8 2022.

[36] L. Li, Y. Li, Q. Du, T. Liu, and Y. Xie, "Ref-nets: Physics-informed neural network for reynolds equation of gas bearing," *Computer Methods in Applied Mechanics and Engineering*, vol. 391, p. 114524, 3 2022.

[37] S. Cuomo, F. Giampaolo, S. Izzo, C. Nitsch, F. Piccialli, and C. Trombetti, "A physics-informed learning approach to bernoulli-type free boundary problems," *Computers and Mathematics with Applications*, vol. 128, pp. 34–43, 12 2022.

[38] N. M. Wilson, A. K. Ortiz, and A. B. Johnson, "The vascular model repository: a public resource of medical imaging data and blood flow simulation results," *Journal of medical devices*, vol. 7, no. 4, 2013.

[39] A. Updegrove, N. M. Wilson, J. Merkow, H. Lan, A. L. Marsden, and S. C. Shadden, "Simvascular: an open source pipeline for cardiovascular simulation," *Annals of biomedical engineering*, vol. 45, no. 3, pp. 525–541, 2017.

[40] L. M. Milne-Thomson and N. Rott, "Theoretical hydrodynamics, fifth edition," *Journal of Applied Mechanics*, vol. 35, pp. 846–846, 1968.

[41] L. Zheng and X. Zhang, "Exact analytical solutions for fractional viscoelastic fluids," *Modeling and Analysis of Modern Fluid Problems*, pp. 279–359, 1 2017.

[42] G. Lu, X. D. Wang, and Y. Y. Duan, "A critical review of dynamic wetting by complex fluids: From newtonian fluids to non-newtonian fluids and nanofluids," *Advances in Colloid and Interface Science*, vol. 236, pp. 43–62, 10 2016.

[43] D. Rubin and E. Krempl, *Introduction to Continuum Mechanics*, 4th ed. Elsevier Inc., 2010.

[44] G. Korn and T. Korn, *Mathematical Handbook for Scientists and Engineers*. Dover Publications, 2000.